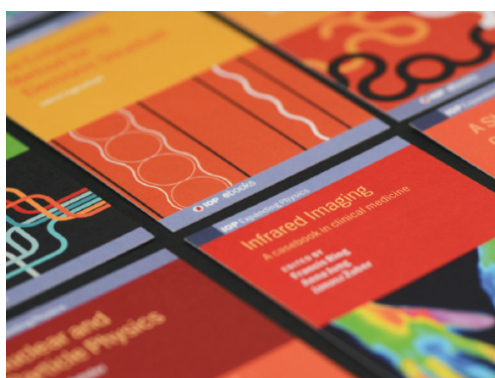


PAPER

Assessment of empirical interatomic potential to predict thermal conductivity in ThO_2 and UO_2

To cite this article: Miaomiao Jin *et al* 2021 *J. Phys.: Condens. Matter* **33** 275402

View the [article online](#) for updates and enhancements.



IOP | ebooks™

Bringing together innovative digital publishing with leading authors from the global scientific community.

Start exploring the collection—download the first chapter of every title for free.

Assessment of empirical interatomic potential to predict thermal conductivity in ThO₂ and UO₂

Miaomiao Jin^{1,*} , Marat Khafizov² , Chao Jiang³, Shuxiang Zhou³,
Chris A Marianetti⁴, Matthew S Bryan⁵, Michael E Manley⁵  and
David H Hurley^{3,*}

¹ Department of Nuclear Engineering, The Pennsylvania State University, 205 Hallowell Bldg, University Park, PA 16802, United States of America

² Department of Mechanical and Aerospace Engineering, The Ohio State University, 201 W 19th Ave, Columbus, OH 43210, United States of America

³ Idaho National Laboratory, 2525 Fremont Ave, Idaho Falls, ID 83402, United States of America

⁴ Department of Applied Physics and Applied Mathematics, Columbia University, New York, NY 10027, United States of America

⁵ Materials Science and Technology Division, Oak Ridge National Laboratory, Oak Ridge, TN 37831, United States of America

E-mail: mmjin@psu.edu and david.hurley@inl.gov

Received 28 November 2020, revised 5 January 2021

Accepted for publication 15 January 2021

Published 28 May 2021



CrossMark

Abstract

Computing vibrational properties of crystals in the presence of complex defects often necessitates the use of (semi-)empirical potentials, which are typically not well characterized for perfect crystals. Here we explore the efficacy of a commonly used embedded-atom empirical interatomic potential for the U_xTh_{1-x}O₂ system, to compute phonon dispersion, lifetime, and branch specific thermal conductivity. Our approach for ThO₂ involves using lattice dynamics and the linearized Boltzmann transport equation to calculate phonon transport properties based on second and third order force constants derived from the empirical potential and from first-principles calculations. For UO₂, to circumvent the accuracy issues associated with first-principles treatments of strong electronic correlations, we compare results derived from the empirical interatomic potential to previous experimental results. It is found that the empirical potential can reasonably capture the dispersion of acoustic branches, but exhibits significant discrepancies for the optical branches, leading to overestimation of phonon lifetime and thermal conductivity. The branch specific conductivity also differs significantly with either first-principles based results (ThO₂) or experimental measurements (UO₂). These findings suggest that the empirical potential needs to be further optimized for robust prediction of thermal conductivity both in perfect crystals and in the presence of complex defects.

Keywords: phonon, thermal conductivity, phonon dispersion, phonon lifetime, density functional theory, empirical interatomic potential

 Supplementary material for this article is available [online](#)

(Some figures may appear in colour only in the online journal)

* Authors to whom any correspondence should be addressed.

1. Introduction

First-principles based modeling of phonon mediated thermal transport using density functional theory (DFT) and the linearized Boltzmann transport equation (LBTE) is a powerful approach for predicting thermal conductivity of crystalline materials [1–5], but it remains too computationally expensive to model crystals with nontrivial defects. Given the much smaller computational cost, molecular dynamics based on empirical interatomic potentials (EIP) provides a path forward for studying thermal transport in the presence of complex defects. Illustrative examples include using the Tersoff potential to examine the influence of vacancy defects on thermal transport in silicon [6], investigating the effect of pores and He bubbles on the thermal transport properties of UO_2 using a composite EIP involving the Leonard-Jones and Buckingham potentials [7], and using the Busker potential to examine the effects of edge dislocations on thermal transport in UO_2 [8].

EIPs are typically trained on data that involves thermo-physical properties such as thermal expansion and specific heat, which are obtained by averaging over the phonons and their interactions. Moreover, these EIPs, and sometimes more advanced machine learning based potentials [9], are widely utilized to model thermal transport without carefully characterizing the vibrational properties of perfect crystals [10–12]. While this training (benchmarking) approach is a good first step, it can lead to scenarios where multiple errors cancel resulting in unfounded confidence in the fidelity of the potential. Another benchmarking approach for EIP involves directly comparing interatomic force constants (IFCs) derived from the EIP to those obtained from first principal calculations. A concern with this approach is that there are far fewer free parameters in the EIP functional formalism than there are unique IFCs, especially third-order IFCs (3IFCs). While it may be argued that only a small subset of 3IFCs are important in deriving thermal transport properties, prediction unencumbered by reduction is desired as it can be compared to measurement with confidence. To directly assess an EIP in the context of thermal transport, one may benchmark EIPs by comparing the prediction of phonon dispersion and lifetime, as well as branch specific conductivity contributions to either experimental measurements or first-principles calculations. Indeed, elements of this approach have recently appeared in the literature for highly characterized materials, such as silicon or gallium nitride [13]. However, significant technological gaps remain for extending this method to more exotic materials that either currently preclude accurate first-principle descriptions or that are difficult to precisely synthesize and/or characterize.

The chemically complex $\text{U}_x\text{Th}_{1-x}\text{O}_2$ system provides an illustrative example in this regard. For the entire compositional spectrum, the phonon properties of this system are a challenge to measure primarily due to the difficulty in growing large single crystal samples suitable for inelastic neutron scattering (INS) measurements. On the uranium-rich side of composition, strong electron correlation effects invalidate conventional first-principles calculations [14]. From this perspective, we consider the efficacy of a popular many-body EIP, developed by Cooper *et al* [15]. This potential (referred

to as CRG) uses the embedded-atom method [16], which incorporates the pair-wise interactions and many-body interactions, with a total of 16 fitting parameters for both ThO_2 and UO_2 systems. These parameters are optimized to reproduce the lattice parameter, the elastic constants, and the thermal expansion coefficient [15]. It exhibits a good reproduction of thermomechanical properties as a function of temperature and composition. It has been extensively used across the chemical compositions from ThO_2 to UO_2 to study thermal transport [10], mass transport [17, 18], radiation damage and defect properties [19, 20]. Further application will involve using this potential to investigate the impact of radiation-induced defects on thermal transport, which has been actively pursued experimentally (e.g., [21–24]). However, a prudent first step should involve testing the efficacy of this potential beyond predicting properties that are obtained by averaging over the phonons and their interactions.

Towards this end, we carefully investigate the phonon structure predicted using this potential—comparing with both detailed experimental results and first-principles calculations. For ThO_2 , we use the second- and third-derivatives of the CRG potential to compute the phonons, phonon linewidths, and the thermal transport within the LBTE, and we make one-to-one comparisons with first-principles calculations and experiments. We find suitable agreement in the phonon dispersion for the acoustic branches, while the highest energy optical branches show considerable disagreement. Additionally, the branch specific contribution to thermal conductivity obtained using the two computation methods exhibits disagreement, most notably for the transverse acoustic (TA) modes. These differences are explored by comparing IFCs and the phonon scattering phase space. For UO_2 , because a first-principles treatment remains elusive due to strong electron correlations, we compare results using the CRG potential to the phonon dispersion curves obtained previously using INS. The disagreement in the overall thermal conductivity and the branch specific conductivity is considered in relation to differences in phonon dispersion and lifetime.

2. Methods

For ThO_2 , we obtain the second-order IFCs (2IFCs) and 3IFCs from the CRG potential and DFT based on the frozen phonon (or small displacement) method. For UO_2 , as DFT has accuracy issues associated with strong electron correlations, only the CRG approach is performed. The forces from the EIP for the displaced supercells are calculated with the LAMMPS package [25]. For DFT, it is as implemented in VASP [26] using the projected augmented wave method [27], and the local density approximation is used to describe the electronic exchange-correlation. The valence electrons for Th and O are 12 and 6, respectively. The conventional cubic unit cell with 12 atoms is fully relaxed, and is used to build supercells. The relaxed lattice constants are DFT- ThO_2 : 5.529 Å, CRG- ThO_2 : 5.580 Å, and CRG- UO_2 : 5.454 Å, respectively. Supercells consisting of $3 \times 3 \times 3$ multiples of conventional unit cells (324 atoms) are generated for 2IFCs calculation (convergence of phonon dispersion

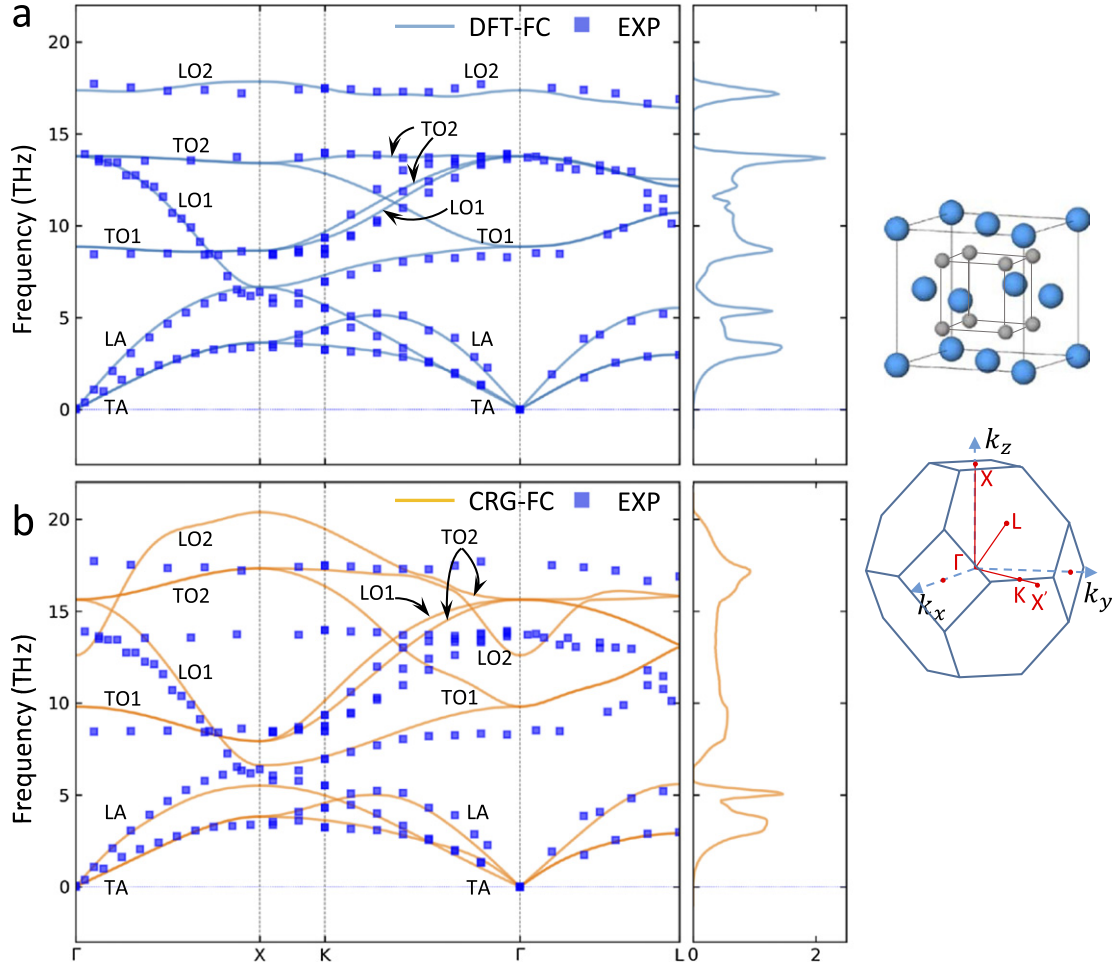


Figure 1. Comparison of dispersion curve and DOS in ThO₂ from DFT-FC and CRG-FC. The experimental measurements [36] (blue squares) are overlapped for comparison. The right figures demonstrate the unit cell structure and the Brillouin zone high symmetry directions.

was tested with respect to supercell sizes). For 3IFCs, supercells consisting of $2 \times 2 \times 2$ multiples of unit cells (96 atoms) are used. The displacement step is set to be 0.03 Å for force evaluation. For the DFT calculations, we used a plane-wave cutoff energy of 650 eV, convergence criterion 1.0×10^{-8} eV in energy, and Monkhorst–Pack k -point grid of $5 \times 5 \times 5$ for $2 \times 2 \times 2$ supercells, and $3 \times 3 \times 3$ grid for $3 \times 3 \times 3$ supercells. The input scripts containing all the relevant settings for the two force calculators are provided in our data repository [28].

Phonopy/phono3py [29, 30] is used to extract IFCs from the EIP and DFT calculations, in addition to predicting dispersion curves and transport properties. The thermal conductivity is calculated using LBTE under the relaxation time approximation (RTA) [31],

$$\kappa_L = \frac{1}{NV_0} \sum_{\lambda} C_{\lambda} \mathbf{v}_{\lambda} \otimes \mathbf{v}_{\lambda} \tau_{\lambda} \quad (1)$$

where N is the number of unit cells in the system and V_0 is the volume of the unit cell. λ denotes the phonon mode as a combination of wave vector and branch index. C_{λ} is the mode heat capacity, \mathbf{v}_{λ} is the phonon group velocity, and τ_{λ} is the phonon relaxation time approximated as the lifetime, which is

the inverse of phonon linewidth [30]. To account for the non-analytical contribution from macro-electric field induced by atomic vibrations [32], the Born effective charge and dielectric constants are included for both approaches. It should be noted that, here we only present the RTA approach as it was demonstrated that the RTA and the full iterative solution of LBTE show very small differences for ThO₂ above room temperature [33]. Furthermore, we found that the conductivity values between the RTA and the direct solution of LBTE [34] as implemented in phono3py [30] are similar. Hence, RTA is adopted throughout this work for computational efficiency and easy interpretation. The convergence with respect to the sampling mesh density in the Brillouin zone was tested [see figure S1 (<https://stacks.iop.org/JPCM/33/275402/mmedia>) in supplementary materials], and the $45 \times 45 \times 45$ mesh grid is used for reporting all the results. The branch specific thermal conductivity is calculated considering all sampling points in the Brillouin zone. This is achieved by projecting the rotated eigenvectors for a general wave vector \mathbf{q} (rotation in accordance with the relation between \mathbf{q} and $\mathbf{q}_{\text{ref}} (\rightarrow \mathbf{0})$) to the branch eigenvectors for \mathbf{q}_{ref} near the Γ point, and then applying weighting factors to the basic phonon branches near the Γ

point (see reference [35] for theoretical formulations). To ease annotation, results obtained using IFCs from DFT calculations will be denoted DFT-FC and results using IFCs from the CRG potential will be denoted CRG-FC.

3. Results

3.1. ThO₂

First, we compare the dispersion curves and density of states (DOS) in ThO₂ for which reliable experimental data exists [36] (figure 1). There are three atoms in the primitive cell, leading to nine branches (three acoustic and six optical branches) with varying degeneracy in the transverse modes across the high-symmetry directions ($\Gamma-X$ [$\xi 00$], $\Gamma-K$ [$\xi \xi 0$], and $\Gamma-L$ [$\xi \xi \xi$]). The dispersion of acoustic branches using DFT-FC and CRG-FC are comparable to recent INS measurements [36] that are reproduced in figure 1. As a result, the DOS below 5.7 THz, corresponding to the acoustic branches, are similar, though there are detectable differences.

The optical branches from DFT-FC agree well with experiment, however, a large discrepancy exists for CRG-FC optical branches. The CRG-FC optical branches exhibit notably larger dispersion, consequently, the DOS lacks well-defined peaks associated with zone boundaries. There are three zone-center frequencies for the optical branches, corresponding to a doubly degenerate TO branch, a triply degenerate Raman-active branch, and a non-degenerate LO branch, respectively [37, 38]. The optical branch zone-center frequencies are [7.9, 13.1, 16.7], [9.8, 15.6, 12.6], and [8.5, 13.7, 17.7] THz for DFT-FC, CRG-FC, and experiment [36], respectively. The LO–TO splitting from the non-analytical term in the CRG-FC approach is much smaller than that from the DFT-FC approach: $Z_{\text{Th}} = 5.404$ (2.2208), $Z_{\text{O}} = 2.702$ (1.1104), where value before (in) the parenthesis is from DFT (CRG). Comparison with/without inclusion of the non-analytical term is provided in the supplementary materials (figures S2 and S3). Notably, a band gap between acoustical and optical branches exists in CRG-FC from 5.7 to 6.6 THz, while there is no gap in DFT-FC.

In figure 2(a), values of κ_L obtained from DFT-FC, CRG-FC, and experiment (EXP) are compared. The DFT-FC and CRG-FC approaches only consider three-phonon processes. Thus, to avoid considering higher order phonon processes that are captured experimentally at high temperatures, a narrow, low temperature range was selected for this comparison. The experimental results, from a previous study on single crystal ThO₂ [39] are included to provide additional perspective. The CRG-FC approach systematically predicts the highest value of κ_L , while DFT-FC provides good agreement with experimental results at the low-temperature end, but gives lower values as temperature increases. Since only three-phonon processes are considered in the BTE model and samples used in experiments always contain defects, it is expected the values for conductivity derived using DFT-FC will be larger than the values obtained experimentally. This discrepancy could relate to multiple factors such as the accuracy in phonon lifetimes (relating to 3IFCs, which are affected by the choice of the

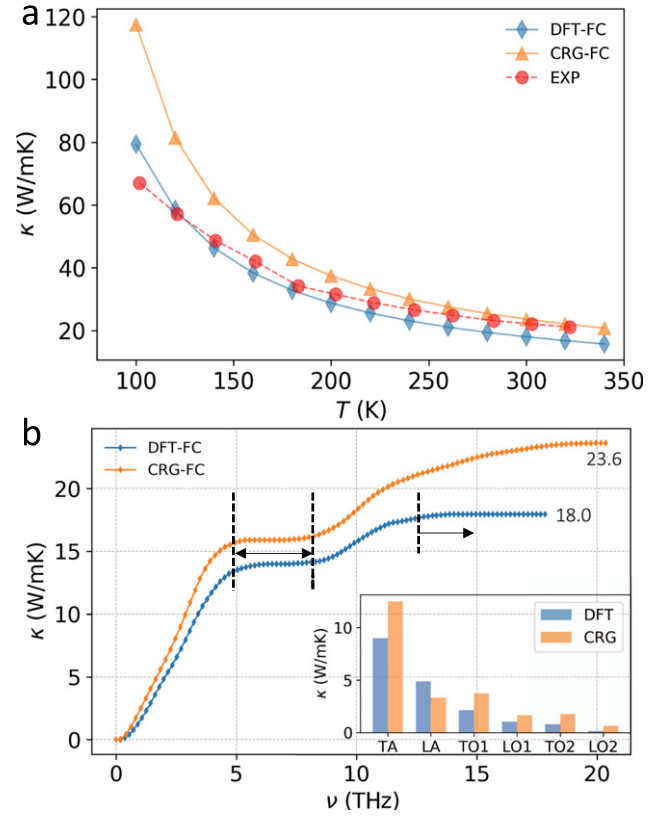


Figure 2. (a) Thermal conductivity with respect to temperature in ThO₂ from DFT-FC, CRG-FC, and experiment (EXP) [39]. (b) Cumulative thermal conductivity vs phonon frequency from DFT-FC and CRG-FC at 300 K. The arrows highlight the frequency range with little contribution to conductivity. The inset indicates the branch specific thermal conductivity.

exchange-correlation functional and simulation cell size), and absence of quartic phonon interactions with thermal expansion. With increasing temperature, CRG-FC indicates better agreement with experiment. It is noted here that extrapolating to 100% theoretical density and correcting for impurity content may move the experimental curve up, especially at low temperatures [40].

Initial insights into factors contributing to the difference in the calculated κ_L can be gained from the analysis of spectral cumulative thermal conductivity κ_L^c , defined as,

$$\kappa_L^c(\omega) = \int_0^\omega \kappa(\omega') d\omega'$$

$$\kappa(\omega) \equiv \frac{1}{NV_0} \sum_\lambda C_\lambda \mathbf{v}_\lambda \otimes \mathbf{v}_\lambda \tau_\lambda \delta(\omega - \omega_\lambda). \quad (2)$$

Figure 2(b) compares conductivity accumulation from DFT-FC and CRG-FC at 300 K. Phonons with frequencies below 5 THz contribute the most in both methods. This frequency range corresponds (figure 1) to acoustic branches. Dashed lines highlight a frequency range with limited contribution to κ_L due to low DOS and/or low group velocities. Conductivity accumulation in DFT-FC reaches a maximum at 13 THz, suggesting that modes above this frequency (mainly the TO2 and LO2 modes) do not directly contribute to thermal transport.

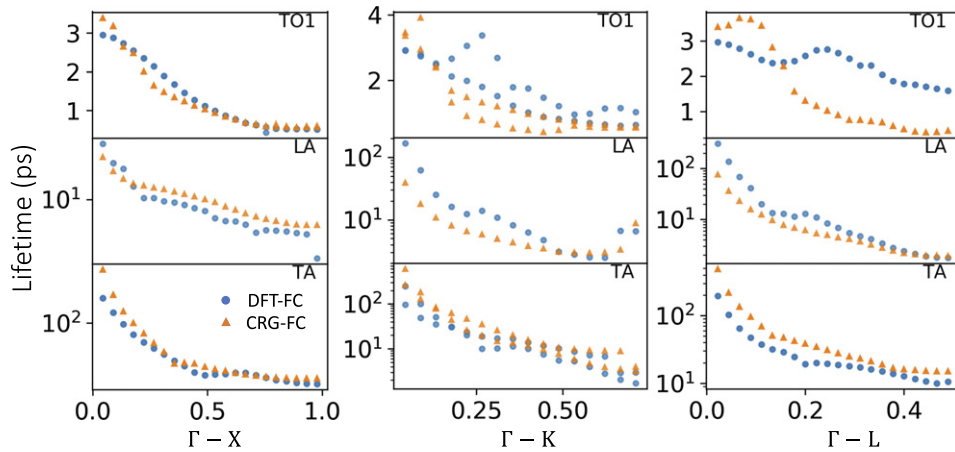


Figure 3. Phonon lifetime for TA, LA, and TO1 modes along Γ -X, Γ -K, and Γ -L from DFT-FC and CRG-FC for ThO_2 at 300 K.

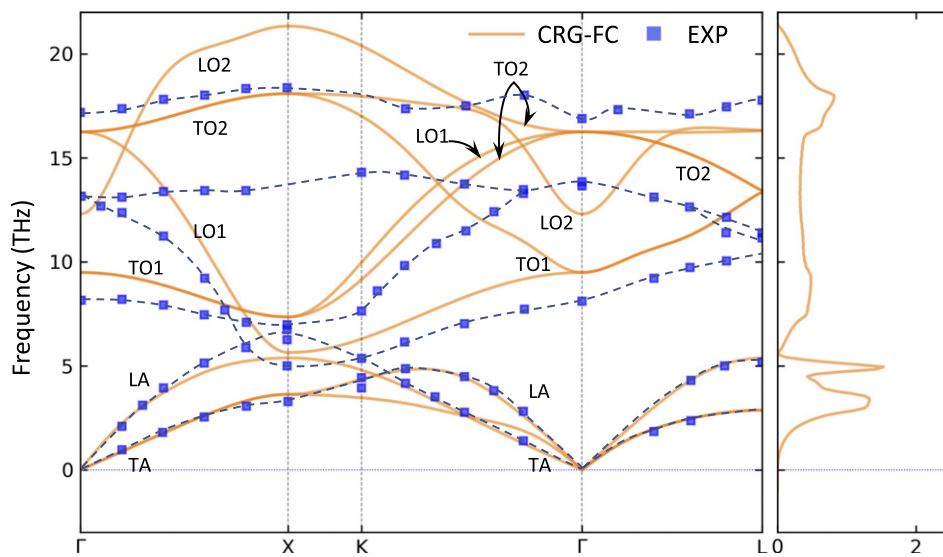


Figure 4. Dispersion curve and DOS in UO_2 from CRG. The experimental measurements [41] (blue squares) are overlapped for comparison. The dashed line is to guide view.

For CRG-FC, on the other hand, κ_L^c continues to increase up until the highest phonon frequency at around 20 THz.

Further perspective is gained by considering the branch specific contribution to conductivity using the projection method (see Methods section). In both cases, transport is dominated by acoustic branches, however the impact of optical branches is non-negligible. The ratios of optical branch contribution to κ_L for DFT-FC and CRG-FC are 23% and 33%, respectively. The difference in acoustic branch contribution is also notable: the TA branch contribution is larger in CRG-FC than in DFT-FC, while the trend is reversed for the LA branch. The phonon lifetimes for the TA, LA, and TO1 branches along three high-symmetry lines are plotted in figure 3. The TA lifetimes are longer in CRG-FC, while DFT-FC leads to slightly longer lifetime phonons for LA and TO1 branches (see supplementary materials figures S7 and S8 for the lifetimes of all modes, and all lifetime vs frequency).

3.2. UO_2

As the CRG potential was developed to cover a wide range of actinide oxides, its capability to describe thermal transport in UO_2 can be similarly examined and compared with experimental results from INS [41]. Here, we do not provide a comparison with DFT calculations, as it was shown by Pang *et al* that DFT simulations for UO_2 fail to accurately describe the details of phonon transport [42]. Figure 4 compares the dispersion curve from CRG-FC with experimental data. The CRG-FC results resemble those for ThO_2 : the acoustic branches exhibit agreement, but the optical modes are pushed to higher energies. The optical branches indicate three zone-center frequencies 9.5, 16.2, and 12.3 THz, in contrast with experimental values 8.1, 13.1, and 17.2 THz from Pang *et al* [41]. The insufficient LO-TO splitting is caused by underestimating the Born effective charge in the CRG potential. Notably, the gap between the acoustic and optical branches becomes minimal compared with CRG-FC results for ThO_2 .

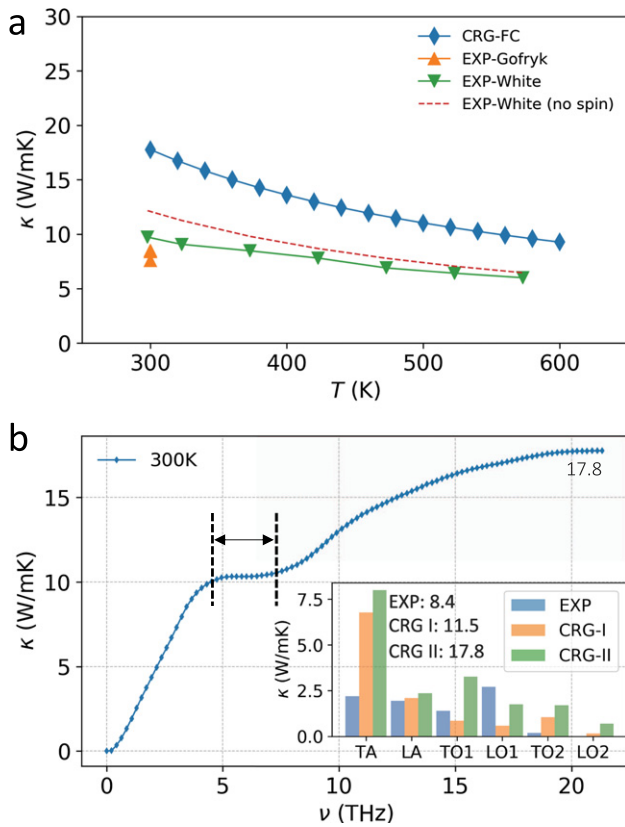


Figure 5. (a) Thermal conductivity with respect to temperature in UO_2 from CRG and experiments (EXP-) [21, 43]. The dashed line is modeling the conductivity without spin scattering using White *et al*'s data. (b) Cumulative thermal conductivity vs phonon frequency from CRG at 300 K. The arrow highlights the frequency range with little contribution to conductivity. The inset indicates the branch specific thermal conductivity from the experiment (EXP), high-symmetry method (CRG-I), and project method (CRG-II).

The thermal conductivity from CRG-FC and the experiments are compared in figure 5(a). CRG-FC exhibits considerably higher conductivity values than experiments. This discrepancy can be partially accounted for by considering phonon-spin scattering (considered in more detail in the next section) [43]. From the cumulative conductivity curve (figure 5(b)), the optical modes contribute around 40% to the total κ_L at 300 K. The inset shows the branch specific thermal conductivity: EXP denotes experimental measurements [41], CRG-I denotes the results calculated using only the high-symmetry directions, and CRG-II includes contribution along all directions. One can see the κ_L is larger by utilizing all the sampling points in the Brillouin zone (11.5 vs 17.8 $\text{W}(\text{mK})^{-1}$). Furthermore, the individual branch contributions to κ_L predicted by CRG-FC differ significantly from experimental results, especially for LO1 where experiment reports a significant contribution to κ_L .

The phonon lifetimes τ using CRG-FC are compared to the measured lifetimes in figure 6 (see supplementary materials figures S8 and S9 for the lifetimes of all modes, and all lifetime vs frequency). The acoustic modes branches obtained from CRG-FC indicate consistency with experimental values, but large lifetimes are found as the wave vector approaches the

zone-center, which is not captured by the experimental measurement. The lifetimes of acoustic phonons generally follow a power law dependence on phonon frequencies, i.e., $\tau \propto \nu^{-n}$, where $n \approx 1.8-2$, consistent with the analysis based on Debye approximation [44].

4. Discussion

In this section, we discuss the differences between prediction based on CRG, DFT and experimental measurements in terms of the 2IFCs and 3IFCs. This discussion is organized into three sections. First, we provide some general discussion regarding phonon dispersion and branch specific contributions to conductivity that is applicable to the ThO_2 and UO_2 systems. Second, we consider in more detail the discrepancy between CRG-FC and DFT-FC for ThO_2 in terms of scattering phase space and phonon scattering strength. Third, for UO_2 we discuss the discrepancy between CRG-FC prediction to experimental measurements of thermal conductivity.

The dispersion curves are determined by the 2IFCs. The CRG potential in general provides a reasonably good description of acoustic branch dispersion curves for both ThO_2 and UO_2 (figures 1 and 4). This is expected considering that this EIP was trained to reproduce elastic constants, which are strongly related to low frequency acoustic branches. However, there is a notable disagreement with the optical branches. From a thermal transport point of view this is important for two reasons. First, in fluorite structures optical branches have been shown to contribute significantly to thermal transport [41]. Second, acoustic-optical phonon scattering is important in limiting thermal transport. The role of 3IFCs and optical branches is revealed when considering the branch specific contribution to thermal conductivity. For ThO_2 , the larger contribution of TA branches for CRG-FC vs DFT-FC (inset in figure 2(b)) is attributed to longer phonon lifetimes (figure 3) despite the fact that dispersion curves are comparable. For ThO_2 , only the LA branch derived from CRG-FC has a smaller contribution as compared with DFT-FC. This is due to shorter lifetimes along $\Gamma-K$ and $\Gamma-L$ directions (figure 3) and noticeably lower energy at the zone boundaries along $\Gamma-X$ direction (figure 1). Similar observations for UO_2 are not possible due to the scarcity of experimental data across the Brillouin zone. For ThO_2 and UO_2 , CRG-FC prediction is consistent in terms of suggesting that optical branches provide a notable contribution to thermal conductivity. However, CRG appears to overestimate the contribution of optical branches. This is attributed to an apparent cancellation of errors where the large velocity of the optical branches is offset by the short lifetimes predicted using CRG-FC (figures 1 and 4). For ThO_2 , because the same level of detail is accessible through the CRG-FC and DFT-FC treatment, it is illustrative to compare individual elements that determine the phonon lifetime.

The three-phonon scattering phase space and scattering strength (based on the 3IFCs), determine the phonon lifetime. The scattering phase space can be quantified via the joint density of states (JDOS) based on conservation of energy and momentum [30]. The selection rules include two classes of three-phonon scattering events, and the total JDOS $D_2(q, \omega)$

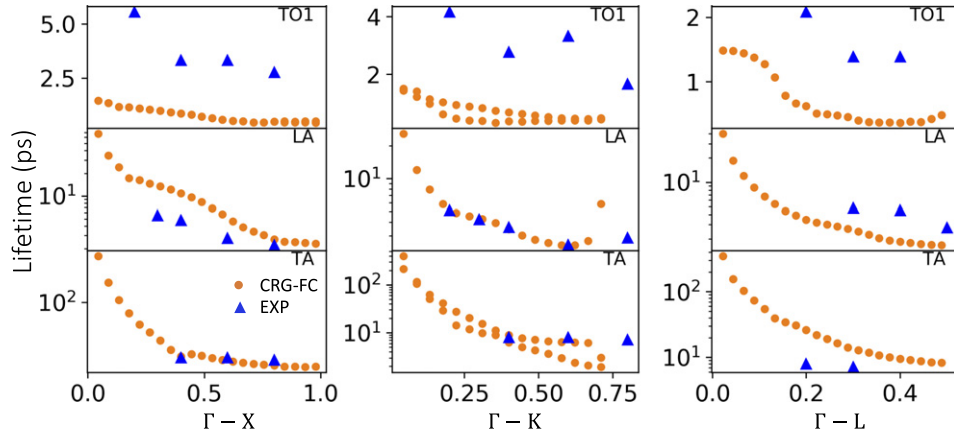


Figure 6. Phonon lifetime for each branch along Γ -X, Γ -K, and Γ -L from CRG and experiment [41] for UO_2 at 300 K.

can be written as a sum of two terms,

$$D_2(\mathbf{q}, \omega) = D_2^{(1)}(\mathbf{q}, \omega) + D_2^{(2)}(\mathbf{q}, \omega), \quad (3)$$

where

$$D_2^{(1)}(\mathbf{q}, \omega) = \frac{1}{N} \sum_{\lambda\lambda''} \Delta(-\mathbf{q} + \mathbf{q}' + \mathbf{q}'') \times [\delta(\omega + \omega_{\lambda'} - \omega_{\lambda''}) + \delta(\omega - \omega_{\lambda'} + \omega_{\lambda''})] \quad (4)$$

$$D_2^{(2)}(\mathbf{q}, \omega) = \frac{1}{N} \sum_{\lambda\lambda''} \Delta(-\mathbf{q} + \mathbf{q}' + \mathbf{q}'') \times \delta(\omega - \omega_{\lambda'} - \omega_{\lambda''}), \quad (5)$$

where the first term corresponds to phonon reactions involving two phonons that scatter into a single phonon and the second term corresponds to a single phonon scattering into two phonons. Herein, \mathbf{q} and ω are the wave vector and angular frequency ($\omega = 2\pi\nu$), respectively. λ represents (\mathbf{q}, j) where j is the band index. The scattering strength can be quantified by defining,

$$P_\lambda = \frac{1}{(3n_a)^2} \sum_{\lambda\lambda''} |\Phi_{\lambda\lambda\lambda''}|^2 \quad (6)$$

where $\Phi_{\lambda\lambda\lambda''}$ denotes the strength of interaction between three phonons ($\lambda, \lambda', \lambda''$) involved in scattering, depending on the 3IFCs [30], and $n_a (=3)$ is the number of atoms in the primitive cell. Figure 7 compares the results of $D_2(\mathbf{q}, \omega)$ and P_λ from DFT-FC and CRG-FC for ThO_2 . For the acoustic phonons (up to $\sim 6\text{THz}$), the scattering phase space predicted using CRG-FC is notably smaller than that predicted using DFT-FC. The primary reason for this is that the optical phonons predicted by CRG-FC are very high in energy and this greatly restricts acoustic to optical scattering processes (similar to materials that exhibit a large phonon bandgap). The scattering strength for the acoustic phonons is comparable for the two methods. This along with the difference in the scattering phase space suggest on average an overestimation of the lifetime of the acoustic phonons. More specifically, consider the peak in the scattering phase space at $\sim 3.8\text{THz}$ which corresponds to frequency band where the TA branches have the highest DOS.

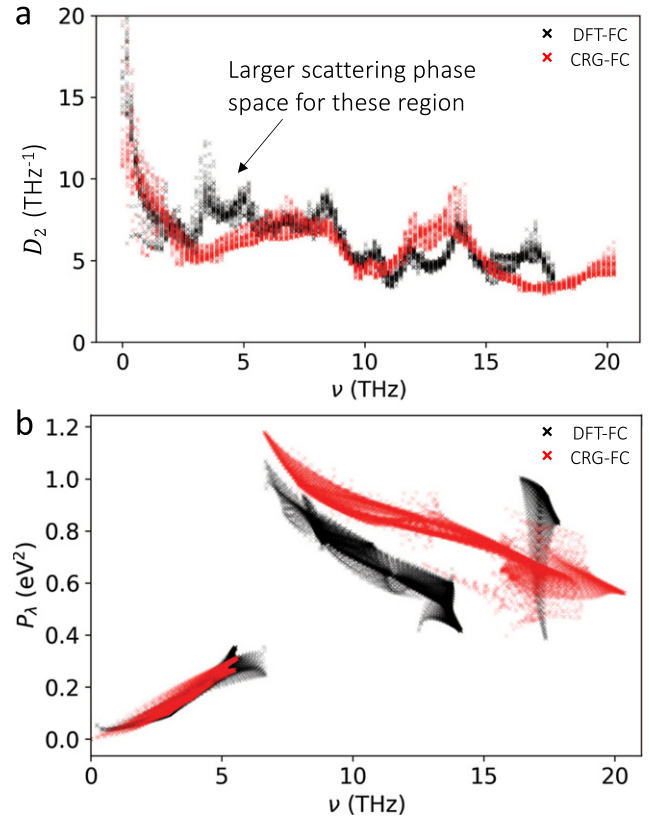


Figure 7. D_2 (a) and P_λ (b) vs frequency ν based on DFT-FC and CRG-FC for ThO_2 .

This observation in combination with the comparable scattering strength are in large part responsible for the significant contribution from the TA branches predicted using CRG-FC.

In UO_2 , our discussion considers a detailed comparison between CRG-FC prediction and experimental measurements of thermal transport. The first step is to consider the impact of anisotropy stemming from the 2IFCs. The second step is to address the influence of resonant spin scattering on limiting values of conductivity at low temperatures.

In the experimental work by Pang *et al* [41], only the high-symmetry direction results (i.e., phonon dispersion and

linewidth) were measured and were used to approximate the whole Brillouin zone. UO_2 exhibits strong elastic anisotropy with a Zener ratio of 0.44 [45]. For the low frequency acoustic branches, this suggests that phonons with wave vectors along low-symmetry (or off-axial) directions may contribute significantly to κ_L . In other words, although the high-symmetry points contain the impact of scattering from all the phonons in the Brillouin zone, the summation in equation (1) needs to properly weight the contribution from the off-axial λ (or \mathbf{q}) points. CRG-I denotes the results calculated using the same method as in the experimental calculations [41], specifically by approximating the whole Brillouin zone using only the high-symmetry sampling points (see reference [41] supplementary materials); and CRG-II indicates the projection method using all \mathbf{q} points. For the branch specific contribution, CRG-I should be compared with experiment as they both only consider high-symmetry directions. For κ_L , CRG-II should be comparable to direct conductivity measurements as both have contributions from phonons propagating along all directions.

Before making this comparison, an additional scattering mechanism must be addressed. For UO_2 , in addition to phonon-phonon scattering, phonons also scatter with unpaired electrons [43, 46]. This is not captured by lattice dynamics. The reduction to the thermal conductivity due to resonant spin scattering has been considered by Liu *et al* [47] using an approach similar to that presented by Gofryk *et al* [43] and it was considered from a purely empirical point of view by Moore *et al* [46]. The reduction in conductivity due to spin scattering calculated by Liu *et al* [47] differs substantially from that estimated by Gofryk *et al* [43] which is most likely due to an underestimation of anharmonicity in [43]. The magnitude of the resonant scattering is large at low temperatures, but with increasing temperature, it diminishes quickly due to an abundance of high frequency phonons that are far removed from the resonant frequency. The empirical approach extrapolates the $1/T$ behavior at high temperatures, observed experimentally, to low temperature to account for the impact of spin scattering. To put things in perspective, the reduction at room temperature due to spin scattering suggested by Gofryk, Liu and Moore is 42 W (mK)^{-1} , 10 W (mK)^{-1} and 2.4 W (mK)^{-1} , respectively. As the approach by Moore *et al* is in keeping with other fluorites [48, 49], this is the approach we used here. The results from this analysis are presented in figure 5(b) as a dashed line. The overestimate of the thermal conductivity by the CRG-FC approach is consistent with the results for ThO_2 . The apparent agreement between CRG-I and the disagreement between CRG-II and experimental measurement of conductivity may be due to a cancellation of errors. To more fully address this supposition will either require accurate electronic structure calculations or more detailed neutron scattering data.

The path forward for both material systems will involve using a more complete picture of the phonons and their interactions to train EIP. This raises an important question: are there enough fitting parameters with the CRG potential to better characterize the phonons and their cubic interactions while retaining existing successes of the CRG potential? Given that the CRG potential has 16 parameters, it seems

possible that the overall behavior may be improved by refitting to phonon properties associated with the 2IFCs and 3IFCs. Furthermore, it would not be difficult to add additional flexibility to the functional form, allowing for more free parameters to improve agreement. One could fit the EIP parameters directly to the quadratic and cubic force constants from DFT. Another promising route involves machine learning algorithms such as neural network interatomic potentials. This approach would involve building datasets from a large quantity of DFT calculations.

5. Conclusion

In summary, the efficacy of the CRG potential for ThO_2 and UO_2 is examined from the perspective of phonon transport properties based on lattice dynamics and LBTE. The phonon dispersion, lifetime, and branch specific thermal conductivity are extensively compared against *ab-initio* based calculations and direct experimental measurements. It is shown that the CRG potential can reasonably capture dispersion of the acoustic branches but exhibits disagreement with the optical branches. For the CRG-FC approach, a bandgap is formed in ThO_2 between the optical and acoustic branches. This gap in addition to the high energy band of the optical phonons leads to a reduction in scattering phase space, longer phonon lifetimes, and a corresponding overestimation of thermal conductivity. For ThO_2 and UO_2 , CRG-FC prediction is consistent in terms of suggesting that optical branches provide a notable contribution to thermal conductivity. This may be attributed to an apparent cancellation of errors where the large velocity of the optical branches is offset by the short lifetimes predicted using CRG-FC. For UO_2 , the apparent agreement between CRG-I and the disagreement between CRG-II and experimental measurement of conductivity may be due to a cancellation of errors. To more fully address this supposition will either require using accurate electronic structure calculations or more detailed neutron scattering data.

Acknowledgments

This work is supported by the Center for Thermal Energy Transport under Irradiation, an Energy Frontier Research Center funded by the U.S. Department of Energy, Office of Science, United States, Office of Basic Energy Sciences. This research made use Idaho National Laboratory computing resources which are supported by the Office of Nuclear Energy of the U.S. Department of Energy and the Nuclear Science User Facilities under Contract No. DE-AC07-05ID14517.

Data availability

The data that support the findings of this study will be openly available following an embargo at the following URL/DOI: <https://doi.org/10.5281/zenodo.4088537>. Data will be available from 20 January 2021.

ORCID iDs

Miaomiao Jin  <https://orcid.org/0000-0002-3543-4082>
 Marat Khafizov  <https://orcid.org/0000-0001-8171-3528>
 Michael E Manley  <https://orcid.org/0000-0003-4053-9986>

References

- [1] Torres E, Cheikhjifon I, Kaloni T P and Pencer J 2020 A comparative analysis of the phonon properties in UO_2 using the Boltzmann transport equation coupled with DFT + U and empirical potentials *Comput. Mater. Sci.* **177** 109594
- [2] Broido D A, Malorny M, Birner G, Mingo N and Stewart D A 2007 Intrinsic lattice thermal conductivity of semiconductors from first principles *Appl. Phys. Lett.* **91** 231922
- [3] Tian Z, Garg J, Esfarjani K, Shiga T, Shiomi J and Chen G 2012 Phonon conduction in PbSe, PbTe, and $\text{PbTe}_{1-x}\text{Se}_x$ from first-principles calculations *Phys. Rev. B* **85** 184303
- [4] Lindsay L, Broido D A and Reinecke T L 2013 *Ab initio* thermal transport in compound semiconductors *Phys. Rev. B* **87** 165201
- [5] Esfarjani K, Chen G and T Stokes H 2011 Heat transport in silicon from first-principles calculations *Phys. Rev. B* **84** 085204
- [6] Lee Y, Lee S and Hwang G S 2011 Effects of vacancy defects on thermal conductivity in crystalline silicon: a nonequilibrium molecular dynamics study *Phys. Rev. B* **83** 125202
- [7] Lee C-W, Chernatynskiy A, Shukla P, Stoller R E, Sinnott S B and Phillpot S R 2015 Effect of pores and He bubbles on the thermal transport properties of UO_2 by molecular dynamics simulation *J. Nucl. Mater.* **456** 253–9
- [8] Deng B, Chernatynskiy A, Shukla P, Sinnott S B and Phillpot S R 2013 Effects of edge dislocations on thermal transport in UO_2 *J. Nucl. Mater.* **434** 203–9
- [9] Behler J and Parrinello M 2007 Generalized neural-network representation of high-dimensional potential-energy surfaces *Phys. Rev. Lett.* **98** 146401
- [10] Cooper M W D, Middleburgh S C and Grimes R W 2015 Modelling the thermal conductivity of $(\text{U}_x\text{Th}_{1-x})\text{O}_2$ and $(\text{U}_x\text{Pu}_{1-x})\text{O}_2$ *J. Nucl. Mater.* **466** 29–35
- [11] Behera R K and Deo C S 2012 Atomistic models to investigate thorium dioxide (ThO_2) *J. Phys.: Condens. Matter* **24** 215405
- [12] Ma J, Zheng J, Wan M, Du J, Yang J and Jiang G 2014 Molecular dynamical study of physical properties of $(\text{U}_{0.75}\text{Pu}_{0.25})\text{O}_{2-x}$ *J. Nucl. Mater.* **452** 230–4
- [13] Rohskopf A, Wyant S, Gordiz K, Reza Seyf H, Gopal, Muraleedharan M and Henry A 2020 Fast & accurate interatomic potentials for describing thermal vibrations *Comput. Mater. Sci.* **184** 109884
- [14] Dorado B, Freyss M, Amadon B, Bertolus M, Jomard G and Garcia P 2013 Advances in first-principles modelling of point defects in UO_2 : f electron correlations and the issue of local energy minima *J. Phys.: Condens. Matter* **25** 333201
- [15] Cooper M W D, Rushton M J D and Grimes R W 2014 A many-body potential approach to modelling the thermomechanical properties of actinide oxides *J. Phys.: Condens. Matter* **26** 105401
- [16] Daw M S and Baskes M I 1984 Embedded-atom method: derivation and application to impurities, surfaces, and other defects in metals *Phys. Rev. B* **29** 6443
- [17] Cooper M W D, Grimes R W, Fitzpatrick M E and Chroneos A 2015 Modeling oxygen self-diffusion in UO_2 under pressure *Solid State Ionics* **282** 26–30
- [18] Cooper M W D, Stanek C R, Turnbull J A, Uberuaga B P and Andersson D A 2016 Simulation of radiation driven fission gas diffusion in UO_2 , ThO_2 and PuO_2 *J. Nucl. Mater.* **481** 125–33
- [19] Rahman M J, Cooper M W D, Szpunar B and Szpunar J A 2018 Primary radiation damage on displacement cascades in UO_2 , ThO_2 and $(\text{U}_{0.5}\text{Th}_{0.5})\text{O}_2$ *Comput. Mater. Sci.* **154** 508–16
- [20] Jin M, Jiang C, Gan J and Hurley D H 2020 Systematic analysis on the primary radiation damage in $\text{Th}_{1-x}\text{U}_x\text{O}_2$ fluorite systems *J. Nucl. Mater.* **536** 152144
- [21] White J T, Nelson A T 2013 Thermal conductivity of UO_{2+x} and U_4O_{9-y} *J. Nucl. Mater.* **443** 342–50
- [22] Pakarinen J, Khafizov M, He L, Wetteland C, Gan J, Nelson A T, Hurley D H, El-Azab A and Allen T R 2014 Microstructure changes and thermal conductivity reduction in UO_2 following 3.9 MeV He_2^+ ion irradiation *J. Nucl. Mater.* **454** 283–9
- [23] Khafizov M, Faisal Riyad M, Wang Y, Pakarinen J, He L, Yao T, El-Azab A and Hurley D 2020 Combining mesoscale thermal transport and x-ray diffraction measurements to characterize early-stage evolution of irradiation-induced defects in ceramics *Acta Mater.* **193** 61–70
- [24] Dennett C A *et al* 2020 The influence of lattice defects, recombination, and clustering on thermal transport in single crystal thorium dioxide *APL Mater.* **8** 111103
- [25] Plimpton S 1995 Fast parallel algorithms for short-range molecular dynamics *J. Comput. Phys.* **117** 1–19
- [26] Kresse G and Furthmüller J 1996 Efficiency of *ab-initio* total energy calculations for metals and semiconductors using a plane-wave basis set *Comput. Mater. Sci.* **6** 15–50
- [27] Kresse G and Joubert D 1999 From ultrasoft pseudopotentials to the projector augmented-wave method *Phys. Rev. B* **59** 1758
- [28] Jin M 2020 Supporting datasets to the current manuscript <https://doi.org/10.5281/zenodo.4088537>
- [29] Togo A and Tanaka I 2015 First principles phonon calculations in materials science *Scr. Mater.* **108** 1–5
- [30] Togo A, Chaput L and Tanaka I 2015 Distributions of phonon lifetimes in Brillouin zones *Phys. Rev. B* **91** 094306
- [31] Srivastava G P 1990 *The Physics of Phonons* (London: Taylor and Francis)
- [32] Gonze X and Lee C 1997 Dynamical matrices, Born effective charges, dielectric permittivity tensors, and interatomic force constants from density-functional perturbation theory *Phys. Rev. B* **55** 10355
- [33] Liu J, Dai Z, Yang X, Zhao Y and Meng S 2018 Lattice thermodynamic behavior in nuclear fuel ThO_2 from first principles *J. Nucl. Mater.* **511** 11–7
- [34] Chaput L 2013 Direct solution to the linearized phonon Boltzmann equation *Phys. Rev. Lett.* **110** 265506
- [35] Cheng L, Zhang C and Liu Y 2019 How to resolve a phonon-associated property into contributions of basic phonon modes *J. Phys. Mater.* **2** 045005
- [36] Bryan M S, Fu L, Rickert K, Turner D, Prusnick T A, Mann M, Abernathy D L, Marianetti C A and Manley M E 2020 Nonlinear propagating modes beyond the phonons in fluorite-structured crystals *Commun. Phys.* **3** 1–7
- [37] Xiao H Y, Zhang Y and Weber W J 2013 Thermodynamic properties of $\text{Ce}_x\text{Th}_{1-x}\text{O}_2$ solid solution from first-principles calculations *Acta Mater.* **61** 467–76
- [38] Malakkal L, Prasad A, Jossou E, Ranasinghe J, Szpunar B, Bichler L and Szpunar J 2019 Thermal conductivity of bulk and porous ThO_2 : atomistic and experimental study *J. Alloys Compd.* **798** 507–16
- [39] Mann M, Thompson D, Serivalsatit K and Tritt T M 2010 Hydrothermal growth and thermal property characterization of ThO_2 single crystals *Cryst. Growth Des.* **10** 2146–51
- [40] Cozzo C, Staicu D, Somers J, Fernandez A and Konings R J M 2011 Thermal diffusivity and conductivity of thorium–plutonium mixed oxides *J. Nucl. Mater.* **416** 135–41
- [41] Pang J W L, Buyers W J L, Chernatynskiy A, Lumsden M D, Larson B C and Phillpot S R 2013 Phonon lifetime investigation of anharmonicity and thermal conductivity of

- UO₂ by neutron scattering and theory *Phys. Rev. Lett.* **110** 157401
- [42] Pang J W L, Chernatynskiy A, Larson B C, Buyers W J L, Abernathy D L, McClellan K J and Phillpot S R 2014 Phonon density of states and anharmonicity of UO₂ *Phys. Rev. B* **89** 115132
- [43] Gofryk K *et al* 2014 Anisotropic thermal conductivity in uranium dioxide *Nat. Commun.* **5** 1–7
- [44] Klemens P G 1958 Thermal conductivity and lattice vibrational modes *Solid State Physics* vol 7 (Amsterdam: Elsevier) pp 1–98
- [45] Fritz I J 1976 Elastic properties of UO₂ at high pressure *J. Appl. Phys.* **47** 4353–8
- [46] Moore J P and McElroy D L 1971 Thermal conductivity of nearly stoichiometric single-crystal and polycrystalline UO₂ *J. Am. Ceram. Soc.* **54** 40–6
- [47] Liu X-Y, Cooper M W D, McClellan K J, Lashley J C, Byler D D, Bell B D C, Grimes R W, Stanek C R and Andersson D A 2016 Molecular dynamics simulation of thermal transport in UO₂ containing uranium, oxygen, and fission-product defects *Phys. Rev. Appl.* **6** 044015
- [48] Pillai C G S and Raj P 2000 Thermal conductivity of ThO₂ and Th_{0.98}U_{0.02}O₂ *J. Nucl. Mater.* **277** 116–9
- [49] Khafizov M *et al* 2014 Thermal conductivity in nanocrystalline ceria thin films *J. Am. Ceram. Soc.* **97** 562–9